Communications to SIMAI Congress,
ISSN 1827-9015, Vol. 1 (2006)
DOI: 10.1685/CSC06036

Inverse Modeling in Geophysical Applications

Daniele Carbone, Gilda Currenti, Ciro Del Negro, Gaetana Ganci, Rosalba Napoli

Istituto Nazionale di Geofisica e Vulcanologia - Sezione di Catania Piazza Roma, 2 95100 - Catania

Abstract
The interpretation of the potential field data is a useful tool that allows for both investigating the subsurface structures and providing a quantitative evaluation of the geophysical processes preceding and accompanying volcanic unrest. Potential fields inversion problem are required to combine forward models with appropriate optimization algorithms and automatically find the best set of parameters that well matches the available observations. Indeed, investigations on the mathematical equations to be inverted have revealed that these models are ill-posed and highly non-linear. Numerical methods for modeling potential fields observations are proposed and applied on real datasets.

Introduction
The inversion problem in potential fields modeling suffers from the ambiguity and instability of its solutions. The ambiguity arises from the inherent property of potential fields for which different combinations of parameters may lead to similar anomalies. Moreover, potential fields inversion is notoriously unstable. Because of ambiguity and instability of solutions, the inversion problem can be secured by narrowing the set of all possible solutions to a predefined solution class that allow for a unique and stable solution. The a priori definition of the geometry (simplified bodies: spherical, rectangular, prismatic) of searched source and the a priori recognition of the involved physical mechanism allows reducing the number of likely solutions considerably (Blakely, 1995). Potential fields inversion method can be classified into two main categories depending on the type of the unknown parameters to be retrieved. Firstly, there are some methods looking for magnetization or density contrast values with fixed geometry sources. In this case linear inversion technique can be successfully applied. Secondly, there are those methods that look for the source geometry . In this latter case the inversion problem is highly non-linear and robust nonlinear inversion techniques are needed. The first category of interpretation models is widely used in providing physical property distributions of subsurface geological structures, while the second one is generally applied in modeling potential fields sources in volcanic areas. In the following two inversion approaches are described to deal with linear and non-linear inversion problems and are applied on two case studies to appraise the goodness of the proposed methods.

3D linear inversion of potential field data
Potential field inversion are aimed to provide a model which reconstructs, as well as possible, subsurface geological structures having a density/magnetization contrast with their surroundings. For the sake of simplicity, we consider the magnetic inverse problem. However, similar formulation can be applied to the case of gravity inversion method. The computational domain V which is supposed to surround the magnetic source is discretized using a finite number of $m = N_x \text{ x } N_y \text{ x } N_z$ rectangular prisms whose magnetization J_j is uniform inside each prism (Blakely, 1995). Using a 3D discrete numerical approach, the total anomaly field at *i-th* observation point is computed by:

$$T_i = \sum_{j=1}^{m} J_j a_{ij} \qquad (1)$$

where elements a_{ij} quantify the contribution to the total anomaly at *i*-th point due to the magnetization of the *j*-th prism (Fedi, 1999). Therefore, the inverse problem can be formulated as the solution of a system of *n* linear equations as:

$$\mathbf{Ax} = \mathbf{T} \tag{2}$$

where **x** is the *m* vector of unknown magnetization values of the prisms, **T** is the *n* vector of observed magnetic data, and **A** is a matrix with elements a_{ij}. The analytical expression of the a_{ij} term for a prismatic body was devised by Rao and Babu (1991). Based on discretization, the number of prisms is usually larger than the number of observation points, thus the linear inverse problem in Eq. (2) turns out to be unavoidably underdetermined. In such a case, the linear system leads to a solution with *m*-*n* degree of freedom. A further difficulty in solving the system in Eq. (2) is due to the inherent non-uniqueness of the potential field: there are an infinite number of inverse models that can explain the same observed magnetic anomaly within error limits. These observations highlight that the magnetic inverse problem is ill-posed. That calls for some regularization techniques. In such a case, it is necessary to impose further assumptions by incorporating a priori knowledge about the solution. The idea of reducing the class of possible solution to some set on which the solution is stable lies on the fundamental concept of introducing a regularizing operator. The inverse problem can be re-formulated as an optimization problem aimed at finding the unknown magnetization values **x** that minimize a data misfit and a smoothing functional:

$$\phi = \frac{1}{2}\left[(\mathbf{Ax} - \mathbf{T}_{obs})^T (\mathbf{Ax} - \mathbf{T}_{obs}) + \lambda(\mathbf{x} - \mathbf{x_0})^T \mathbf{W}^T \mathbf{W}(\mathbf{x} - \mathbf{x_0})\right] \tag{3}$$

where W is a weighting matrix. To ensure that the solution is geologically reasonable it is advisable to prescribe realistic bounds on the magnetization values on the basis of rock samples or available information about the local geology. The minimization of the quadratic functional in Eq. (3) subjected to bound constraints can be solved by using a Quadratic Programming (QP) algorithm based on active set strategy (Gill et al., 1991):

$$\min\phi = \min\left[\frac{1}{2}\mathbf{x}^T\mathbf{Q}\mathbf{x} - \mathbf{d}^T\mathbf{x}\right], \quad \mathbf{L} \le \mathbf{x} \le \mathbf{U} \tag{4}$$

where $\mathbf{Q} = \mathbf{A}^T\mathbf{A} + \lambda\mathbf{W}^T\mathbf{W}$ and $\mathbf{d} = \mathbf{A}^T\mathbf{T} + \lambda\mathbf{W}^T\mathbf{W}\mathbf{x_0}$, and **L** and **U** are the vectors of lower and upper bounds. The quadratic formulation of the problem is solved iteratively by generating a sequence of feasible solutions that converge toward the optimal solution. The iteration is stopped when no relative improvements in the functional are achieved. QP algorithm was applied to analyze the anomalies detected by a high resolution ground magnetic survey of the Ustica island. The total-intensity anomaly field, obtained after data reduction process, shows the presence of a W-E striking magnetic anomaly in the middle of the island and other two intense anomalies, which seem to continue offshore, in the south-western and the north-eastern sides (Fig. 1). In order to allow the maximum flexibility for the model to represent geologically realistic structures the island was represented as a crustal block, 4x3 km^2 area and about 1.2 km thickness, and was discretized into a set of rectangular prisms (0.125 x 0.125 x 0.15 km^3 in size) whose magnetization values are allowed to vary in the range of 0-10 A/m. The 3D model reveals the presence of three main magnetic trends, N-S, E-W and NE-SW, which are coincident with the main regional structural lineaments (Fig. 2). In particular, the N-S and E-W trends, which are of more recent origin, prevail in the shallow part of the model, while the NE-SW is relevant below 0.4 km b.s.l. At this depth the model reveals a magnetized body in the central area, which may be interpreted as the preferential area for magma storage and ascent and which supplied the feeding systems of the main subaerial volcanic centers of the island. Two other magnetized volumes were identified and ascribed to the small submarine/subaerial eruptive centers of the western island and to the younger cone of Capo Falconiera, respectively. These findings highlight how the regional tectonics has strongly influenced the structural and magmatic evolution of the Ustica volcanic complex producing preferential ways for magma ascents.

Non-linear inversion of gravity anomaly by genetic algorithm technique

The inversion problem of potential fields anomalies preceding and accompany volcanic eruptions deals with the identification of the parameters of a volcanic source that causes observable changes in data recorded in volcanic areas. Investigations on the analytical solutions have revealed that the involved models are highly non-linear and characterized by several parameters. When non-linear models are involved, the inverse problem becomes difficult to solve through local optimization methods. We have investigated the use of Genetic Algorithms (GAs; Currenti et al., 2005) which perform a broad search over the parameters space with the aim of minimizing an objective function that quantifies the misfit between model values and observations. The GAs inversion strategy was applied on a gravity anomaly that grew up in 5 months before the 2001 eruption of Mt. Etna along a East-West profile of stations (Carbone et al., 2003). Between January and July 2001, the amplitude of the change reached 80 μGal, while the wavelength of the anomaly was of the order of 15 km. Elevation changes observed through GPS measurements during a period encompassing the 5-month gravity decrease, remained within 4-6 cm all over the volcano and within 2-4 cm in the zone covered by the microgravity profile. We review both gravity and elevation changes by a model assuming the formation of new cracks, uniformly distributed in a rectangular prism (Okubo and Watanabe, 1989). This model implies inversion for nine parameters, m = {A, X, Y, Z_1, Z_2, L, W, U, $\Delta\rho$} (Table 1). To make the GA converge towards a solution which (i) best fits the observed data and (ii) has a good chance to be realistic from the volcanological point of view, we suitably restrict the parameter space to be investigated. The ranges of model parameters are set on the grounds of the available geophysical and geological evidence.

Parameter	***Minimum***	***Maximum***	***Best value***
Z_1 - Depth of the top (m b.s.l.)	0	2500	409
L - Length (m)	1000	5000	5000
H - Height (m)	3000	7000	7000
W - Thickness (m)	500	2000	500
A - Azimuth (from the North)	-45	0	-30
X - Northing Coordinate(m)	4170000	4180000	4173940
Y - Easting Coordnate(m)	495000	505000	503499
$\Delta\rho$ - Density contrast (kg/m^3)	-2400	-2700	-2500
U - Extension (m)	0	2	2

Table 1. The best model parameters found by the GA.

For the inversion procedure, we have set the objective function equal to the value of chi-square that accounts for the measurements error defined by the standard deviation σ, as:

$$\chi^2 = \sum_k \frac{(M_k - C_k)^2}{\sigma_k^2} \tag{5}$$

where M_k are the measured data, C_k are the computed gravity variations and k is the number of available measurements. The best model parameters found through the GA are reported in Table I. The fit between observed and calculated gravity gives a residual of 7.43 μGal (Fig. 4), well within the error on temporal gravity differences (10 μGal at the 95% confidence interval). Results show that, although the observed gravity changes are explained by the proposed model, calculated elevation changes are significantly higher than observed. This finding could imply that either (a) the elastic half-space assumption of the Okubo model is fallacious at Etna at the inferred depth, where tectonic and lithologic discontinuities could make the medium heterogeneous or (b) another mechanism, allowing a significant density decrease without deformation, coupled the Okubo's model or acted instead of it, increasing the gravity effect while leaving the displacements at the surface unchanged. A finite element method could be implemented to take into account the effect of medium heterogeneities, and test whether it is

reasonable to postulate that the total volume of new voids, needed to explain the observed gravity decrease, can be accommodated at depth with an ensuing small deformation at the surface. As for the second hypothesis, the only mechanism allowing a density decrease at depth without surface displacements is empting of a magma reservoir. To keep the maximum elevation change within 2-4 cm, a value of U equal to about 1 m should be assumed. Using this value for the extension of the fracture zone and the best values found by the GA for the other parameters (Table 1), only about 50% of the observed gravity decrease can be explained. Under the assumption that the inferred source-volume contains both the new-forming infinitesimal cracks and the empting reservoir(s), it results that an about 10^{11} kg mass should be lost from the inferred source volume to contribute the missing 50% of the observed gravity decrease. The inferred mass corresponds to a minimum volume of magma of $35*10^6$ m^3. It is interesting to note that, during late 2000 and the first months of 2001, an almost continuous activity, with lava emission and Strombolian explosions from the summit Southeast Crater, was observed (Lautze et al., 2004). The volume of the products emitted between January 2001 and the start of the main flank eruption is estimated to range between 13 and $20*10^6$ m^3, and thus is of the same order of magnitude as the volume lost from the inferred source, following the above calculation.

Conclusion

Two procedures dealing with linear and non-linear inversion of potential field data were applied. Although the inversion problem suffers from the ambiguity and instability of its solutions, numerical methods allow for narrowing the set of all possible solutions and providing a unique and stable solution. As for large-scale linear inverse problem, a 3D inversion of magnetic field data was performed by means of QP algorithm to produce a magnetization model that provides useful information of the subsurface geological structure of Ustica volcanic complex. As for non-linear potential fields inversion, a GA technique was proposed to infer the parameters of a volcanic source that causes the growth of a negative gravity anomaly preceding the 2001 Etna eruption. Our findings demonstrate that the identification and interpretation of potential field data can be a useful instrument both for detecting subsurface geological structure model and improving the monitoring of active volcanoes.

Bibliography

Blakely, R. J., 1995. Potential Theory in Gravity and Magnetic Applications, Cambridge University Press, New York, 435 pp.

Carbone D, Budetta G, Greco F (2003) Bulk processes some months before the start of the 2001 Mt Etna eruption, evidenced throught microgravity studies. J Geoph Res 108(B12), 2556, doi:10.1029/2003JB002542.

Currenti G, Del Negro C, Nunnari G (2005b) Inverse modelling of volcanomagnetic fields using a genetic algorithm technique. Geophys J Int 162: 1–16.

Fedi, M., Rapolla, A., 1999. 3-D inversion of gravity and magnetic data with depth resolution. Geophysics, 64, 452-460.

Gill, P.E., Murray, W., Ponceleon, D.B., Saunders, M., (1991) Solving reduced KKT systems in barrier methods for linear and quadratic programming. Technical Report SOL 91–7, Stanford University, Stanford, CA.

Lautze NC, Harris AJL, Bailey JE, Ripepe M, Calvari S, Dehn J, Rowland SK, Evans-Jones K (2004) Pulsed lava effusion at Mount Etna during 2001. J Volcan Geotherm Res 137: 231– 246

Okubo S, Watanabe H (1989) Gravity change caused by a fissure eruption. Geophys Res Lett 16: 445-448.

Rao, D. B., Babu, N. R., (1991) A rapid method for three-dimensional modeling of magnetic anomalies. Geophysics. VOL. 56. NO. II (November 1991), 1729-1737.

Figure

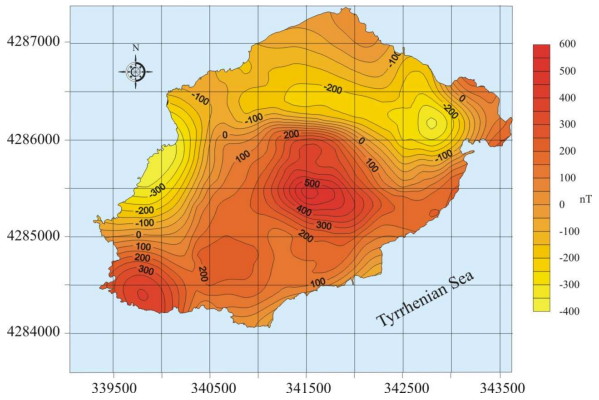

Fig. 1 – Map of the total intensity magnetic field after reduction process.

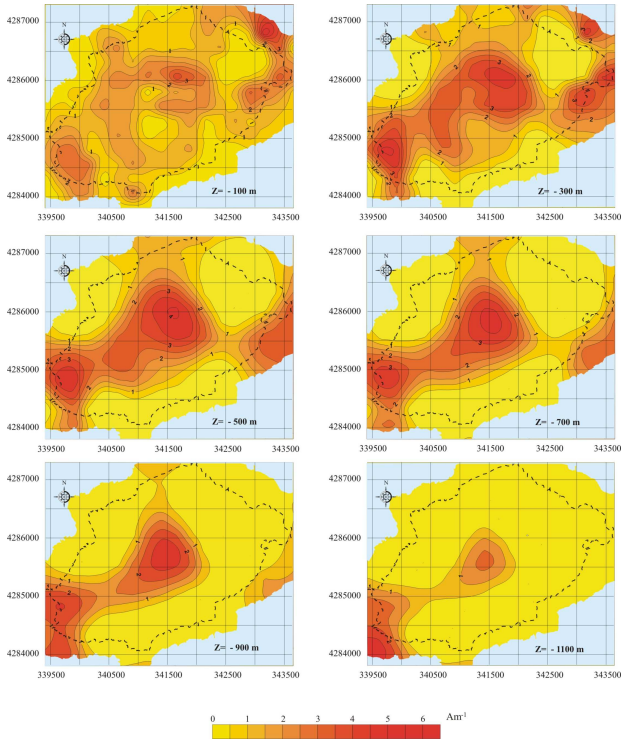

Fig. 2 – The 3 D magnetization model of the Ustica volcanic complex. Horizontal sections of the uppermost part (above sea level) of the model (a) and from 100m depth until 1100m depth (b to g).

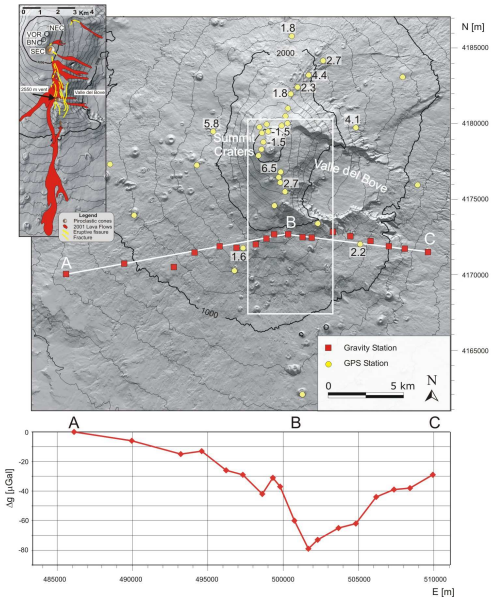

Fig. 3 - Sketch map of Mt. Etna. Top: the gravity stations of the microgravity network along the East-West Profile (ABC) and the GPS stations measured in July 2000 and June 2001. The elevation changes higher than 1.5 cm, observed during the same interval, are also reported. The inset on the left shows the 2001 lava flow. Bottom: gravity change observed between January and July 2001 along the East-West Profile.

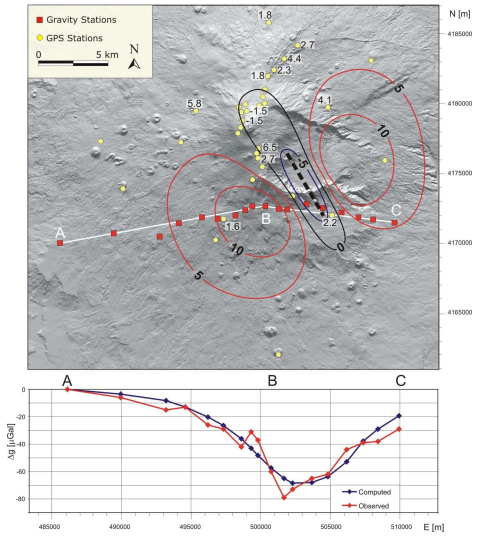

Fig. 4 - Results based on the best model. Top: contour map (at 5 cm intervals) of computed elevation changes; surface projection of the source (dashed line); observed (July 2000 - June 2001) elevation changes higher than 1.5 cm. Bottom: observed (January - July 2001) and computed gravity anomalies.